Title
Seismic response of retaining walls with cohesive backfill: Centrifuge model studies

Authors
Candia, Gabriel
Mikola, Roozbeh Geraili
Sitar, Nicholas

Publication Date
2016-11-01

DOI
10.1016/j.soildyn.2016.09.013

Peer reviewed

Seismic response of retaining walls with cohesive backfill: Centrifuge model studies

Gabriel Candia[a,b,*], Roozbeh Geraili Mikola[c], Nicholas Sitar[d]

[a] Facultad de Ingeniería at Universidad del Desarrollo, Chile [b] National Research Center for Integrated Natural Disaster Management CONICYT/FONDAP/15110017, Chile [c] McMillan Jacobs Associates, San Francisco, CA, USA [d] Department of Civil and Environmental Engineering, University of California Berkeley, Berkeley, CA, USA

* Corresponding author. E-mail address: gcandia@udd.cl (G. Candia).

Abstract

Observations from recent earthquakes show that retaining structures with non-liquefiable backfills perform extremely well; in fact, damage or failures related to seismic earth pressures are rare. The seismic response of a 6-m-high braced basement and a 6-m free-standing cantilever wall retaining a compacted low plasticity clay was studied in a series of centrifuge tests. The models were built at a 1/36 scale and instrumented with accelerometers, strain gages and pressure sensors to monitor their response. The experimental data show that the seismic earth pressure on walls increases linearly with the free-field PGA and that the earth pressures increase approximately linearly with depth, where the resultant acts near 0.33 H above the footing as opposed to 0.5–0.6 H, which is suggested by most current design methods. The current data suggest that traditional limit equilibrium methods yield overly conservative earth pressures in areas with ground accelerations up to 0.4*g*.

Keywords: Centrifuge tests, Retaining walls, Seismic earth pressures, Mononobe-Okabe

1. Introduction

Despite being a broad simplification of what, in reality, is an extremely complex soil-structure interaction problem, the most commonly used approach to seismic analysis and design of retaining structures is the Mononobe-Okabe method (M-O). This method was developed by Okabe [1] and Mononobe and Matsuo [2] following the great Kanto earthquake of 1923 that devastated many retaining structures, particularly the quay walls in Yokohama Harbor. Their method, i.e., a Coulomb wedge limit equilibrium (LE) analysis, drew on the results of pioneering shaking-table experiments conducted by Mononobe and Matsuo [2]. Their model was a rigid box filled with dry loose sand subjected to harmonic motions. The total seismic load was measured using pressure gauges and resulted in excellent agreement with Okabe's general theory of earth pressure [1].

Since then, much research has been conducted on the seismic response of retaining walls, and generally, these studies suggest that the M-O theory is appropriate for low levels of ground accelerations. Other LE methods, e.g. [3–

8], improved on Okabe's general theory to account features such as surface cracks, wall-tosoil adhesion, the backfill flexibility, inertial body forces, and logspiral failure surfaces among others. Most of these solutions, however, lack of experimental data at large accelerations and the evaluation of the critical failure surface typically requires a numerical solution. Likewise, kinematic solutions [9] and methods based on the theory of elasticity have been developed [10–14], but their applicability is limited since a small wall deflection can induce a failure state in the soil. Finite elements or finite differences models have been used extensively to analyze retaining structures [15–20]. While these methods have been validated against real case histories and experimental data, their predictive capabilities is still debatable.

A number of experimental studies have been conducted to substantiate the magnitude of earth pressures on retaining walls, since the early work of Okabe [1] and Mononobe and Matsuo [2]. Recent experimental evidence [20–23] and the observed field performance [24–26] show that M-O theory yields very conservative designs in areas where the peak ground acceleration (PGA) exceeds 0.4*g*. Among other reasons, classic methods of analysis overestimate the seismic earth pressures on retaining walls because the cohesive strength of the soil is typically ignored and the models assume an infinitely rigid backfill [27].

In general, the experimental data fall into two categories: small-scale 1-*g* shaking-table experiments and geotechnical centrifuge experiments. The 1-*g* shaking-table experiments that were prevalent in the past, e.g., [28–32], produced seismic loads consistent with M-O theory; however, in general, these experiments suggested that the earth pressure resultant acts at a point higher than H/3. As a result, the line of action of the dynamic force was typically chosen to be between 0.6 and 0.67 H [e.g., 33]. However, an important limitation of scaled 1-*g* shaking-table experiments is that even with the most careful scaling, the soil response cannot be easily scaled to prototype dimensions because the strength and stiffness of the soil, which control the soil behavior, are nonlinear functions of the confining stress. In addition, shaking table models built in rigid boxes on a rigid base do not reproduce the boundary conditions encountered in field settings, and the models are typically limited to short walls, i.e., typically less than 2 m in height, founded on stiff rock and retaining a medium loose soil.

While not completely devoid of scaling problems, centrifuge tests allow for correct scaling of stresses and strains in the soil [34]. The earliest centrifuge model of the seismic response of retaining structures was reported by Ortiz et al. [35], who studied the response of flexible cantilever walls in medium-dense sand. The container was subjected to earthquake-like motions, which resulted in seismic pressures consistent with M-O theory, and a seismic resultant located at 1/3 H. Bolton and Steedman [36,37] studied the centrifuge response of micro concrete cantilever walls that retained a dry cohesionless backfill. The walls were fixed to the loading frame and were

subjected to harmonic accelerations up to 0.22*g*. The results suggested that the wall inertial forces must be taken into account in addition to M-O earth pressures.

Later, Dewoolkar [38] modeled the centrifuge response of liquefiable backfills on fixed-base cantilever walls under harmonic accelerations and showed that excess pore pressure and inertial effects contributed significantly to the total seismic lateral pressure. Nakamura [39] modeled the centrifuge response of free-standing gravity walls retaining dense Toyura sand (Dr = 88%). The author showed that a ‘soil wedge’ forms in the backfill and slides down plastically during the earthquake, i.e., plastic strain accumulate in the slip plane when the soil is loaded in both (active and passive) directions. In contrast, the response implied by M-O theory suggests that the soil wedge that follows the retaining structure moves down when loaded in the active direction and moves up when loaded in the passive direction. Additionally and contrary to M-O theory, the author observed that the earth pressure distribution is nonlinear, changes over time, and is a function of the type of ground motion used. Nakamura observed complex interaction patterns between the backfill and wall, and concluded that even in controlled environments, the underlying assumptions of M-O theory are generally not met.

More recently, Al Atik and Sitar [20] and Sitar et al. [21] modeled the seismic behavior of fixed-base U-shaped walls, basement walls and free-standing cantilever walls supported in medium-dense sand. The experiments used a flexible shear beam container that deforms horizontally with the soil. The authors concluded that the M-O method was conservative, particularly when PGA>0.4*g*, providing further support to the Seed and Whitman's [33] observation that properly designed retaining walls should be capable of withstanding 0.3*g*. The authors also observed that seismic earth pressure increased approximately linearly with depth and that the Seed and Whitman [33] method with the resultant applied at 0.33 H is a reasonable upper bound to the total seismic load. However, while the past experimental work has been devoted almost exclusively to cohesionless backfills, many backfills are made of compacted soil or natural soil deposits that have a certain degree of cohesion that may significantly reduce the loading demands on the system [6,40,41]. Thus, this study was motivated by the lack of experimental data on the seismic response of retaining structures with cohesive backfills. The experimental program was conducted at the NEES Center for Geotechnical Modeling (CGM) and consisted of scaled centrifuge models of free-standing cantilever walls and basements walls with a level backfill. The numerical simulation of these centrifuge tests was performed in FLAC-2D and will be the subject of another article.

2. Centrifuge model

The primary advantage of centrifuge experiments over 1-*g* shaking-table experiments is the correct scaling of the stressstrain behavior in the soil,

which enables the model to reproduce the behavior of full-scale prototypes. A thorough discussion of the centrifuge scaling principles can be found elsewhere [34]. Nevertheless, centrifuge models are not problem free: the gravitational field increases with depth; highly sensitive instruments are required to capture the frequency content of centrifuge earthquakes; and there are no stationary reference points because undesired vibrations develop in the loading frame as a result of the dynamic interaction with the soil model. The latter becomes an issue when there is mass asymmetry within the soil. The large centrifuge at CGM has a 9-m radius with a payload of 4.5 t at 75*g*'s of gravity (Fig. 1a). A 1-D shaking table mounted on the centrifuge arm reproduces earthquake-like ground motions and delivers a PGA between 20*g* and 30*g*, which is equivalent to 0.4*g* and 0.6*g* if a scaling factor of N=50 is used, respectively. In the present study, the models were built in a flexible shear beam (FSB) container (Fig. 1b), which deforms horizontally with the soil and helps simulate free-field conditions during earthquakes. Multiple sensors were used in the experiment; data were collected at a rate of 4096 Hz using a high-speed Data Acquisition system.

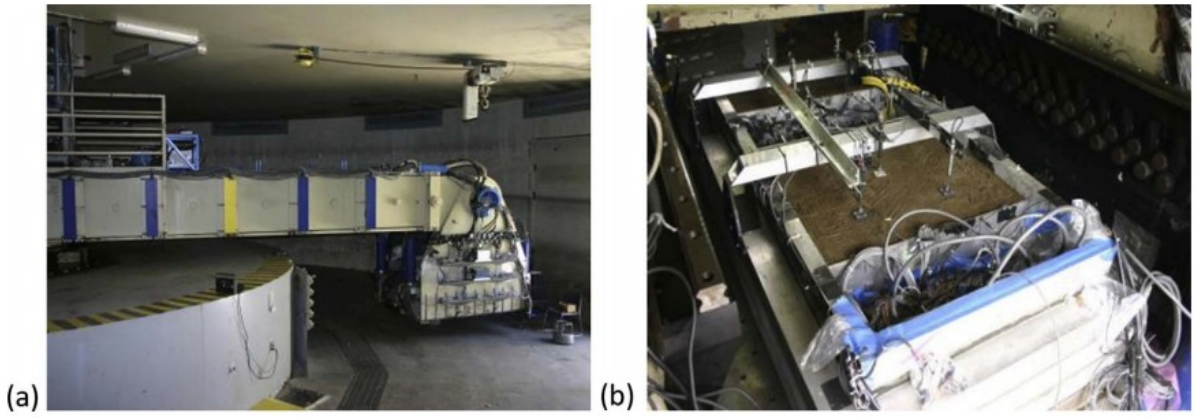

Fig. 1. (a) CGM's centrifuge at rest, and (b) centrifuge model in the arm.

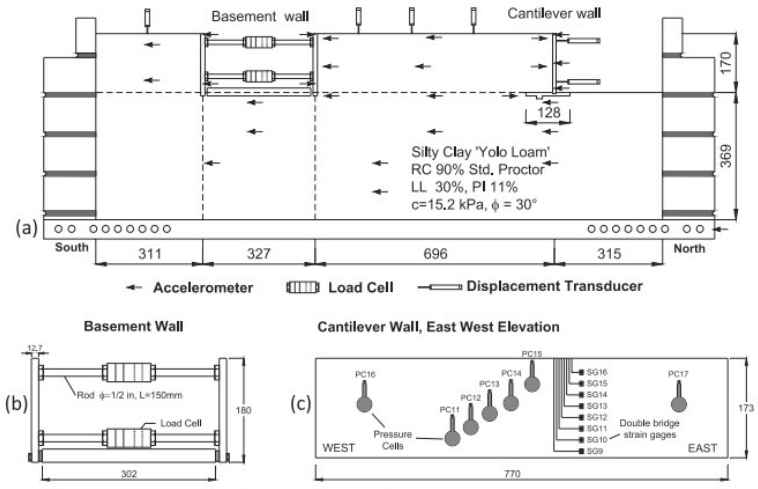

Fig. 2. (a) Experimental setup: FSB container, soil, and structures, (b) basement wall elevation, (c) pressure cells and strain gages on cantilever wall. All dimensions in mm.

3. Experiment design

An embedded one-story basement wall and a free-standing cantilever wall were modeled in the centrifuge with a scaling length factor of 1/36 and tested at 36*g* of centrifuge acceleration. The full-scale prototypes were 6-m-high reinforced concrete (RC) structures underlain by 13 m of clay and spaced 25 m from each other to minimize interaction effects. The model width was 28 m and the ground motions were applied in the direction perpendicular to the walls. The retained soil consisted of a 6-m-deep compacted clay, as shown in Fig. 2(a). The basement consisted of two walls built with 12.7-mm-thick aluminum plates and a bottom slab built with 25.4 mm-thick aluminum plates. In order to measure the static and seismic lateral earth pressures, the opposing walls were connected through six cross bracings instrumented with load cells. Although the basement configuration produced a laterally stiff structure, it did not entirely eliminate racking. The prototype cantilever wall was a standard AASTHOLRFD retaining wall per Caltrans specifications, which has a wide footing and a shear key to prevent rigid body sliding. To match the effective moment of inertia of the prototype RC wall, the model components were built with 9.5-mm-thick aluminum plates.

The soil used in the experiment was a lean clay, Yolo Loam (LL=30%, PI=11%, ω_{opt}=15%). The foundation soil and the retained soil layers were compacted in 25.4 mm lifts at a relative compaction effort equivalent to 90% standard Proctor at a moisture content of 17%, which resulted in a dry unit weight of 16.5kN/m^3.

Strength parameters c=15.2 kPa and φ=30° were interpreted from a series of triaxial compression tests on un-saturated samples obtained from a depth of 350 mm at the middle span after the centrifuge tests was completed. The samples (with average height 15 cm and average diameter 7.4 cm) were confined isotropically at 50, 100, 150, and 200 kPa, and sheared until failure at a rate of 0.5 mm/min. These confining pressures correspond to depths 4.4 m, 8.8, 13.2, and 17.6 m in prototype scale.

The shear wave velocity at a confining stress of 100 kPa was estimated between 175725 m/s based on resonant column tests (ASTM D4015) using bender elements within the soil model. The measured shear strain versus shear modulus reduction curves agreed with the published relationships for low-plasticity soils [42,43]. Approximately 80 instruments were used to monitor different physical parameters in the soil and structures, including the following: accelerometers, displacement transducers, pressure cells, load cells in the basement walls, and strain gages on the cantilever wall. The approximate locations of the instruments are shown in Fig. 2(b) and (c).

Nine ground motions from three different earthquakes were used in the experiment to study the dynamic response of the system. These ground motions were previously scaled and filtered [20] to fit the capabilities of the shaking table mounted on the centrifuge while preserving the primary

characteristics of the original ground motions. A comparison between the response spectra of four original records obtained from the PEER database and the simulated centrifuge motions is presented in Fig. 3. To account for previous seismic history and the cumulative displacement of the retaining structures, the loading protocol was defined such that the ground motion intensity was increased from medium to strong and then reversed.

4. Test results

The PGA of the backfill and structures is shown in Fig. 4 as a function of the input intensity. The input acceleration was deamplified at the foundation level as a result of energy dissipation in the soil; likewise, the ground motion at the free surface was reduced for input PGA>0.3*g*, which is consistent with typical ground amplification charts for medium-clayey soils [44]. The ground motion at the top of the walls was amplified, which was more significant at the top of basement wall, possibly due to the inertial coupling with the flexible container.

The profiles of the relative ground acceleration and relative ground displacement in Fig. 5 show that the model responded primarily in the first and second modes. The influence of higher modes was evaluated using modal composition [45] as follows:

$$u(z) = \sum_n \psi_n U_n(z) \qquad (1)$$

where $U_n = \cos(\pi z(2n-1)/2H)$ is the n-th vibration mode of a uniform soil deposit, and ψ_n is the corresponding amplification factor. The analysis shows that on average, over 85% of the total displacement comes from the first mode, 12% from the second mode, and less than 3% from higher modes.

The elastic response spectra with 5% damping are shown in Fig. 6 for the input motion and free-field motion at the ground surface. The plots show that for low levels of shaking, e.g., Kocaeli, the pseudo accelerations at all natural periods were amplified, whereas in stronger motions, e.g., Loma Prieta and Kobe, the ground response was reduced at short periods (T<0.4 s) and amplified at larger periods.

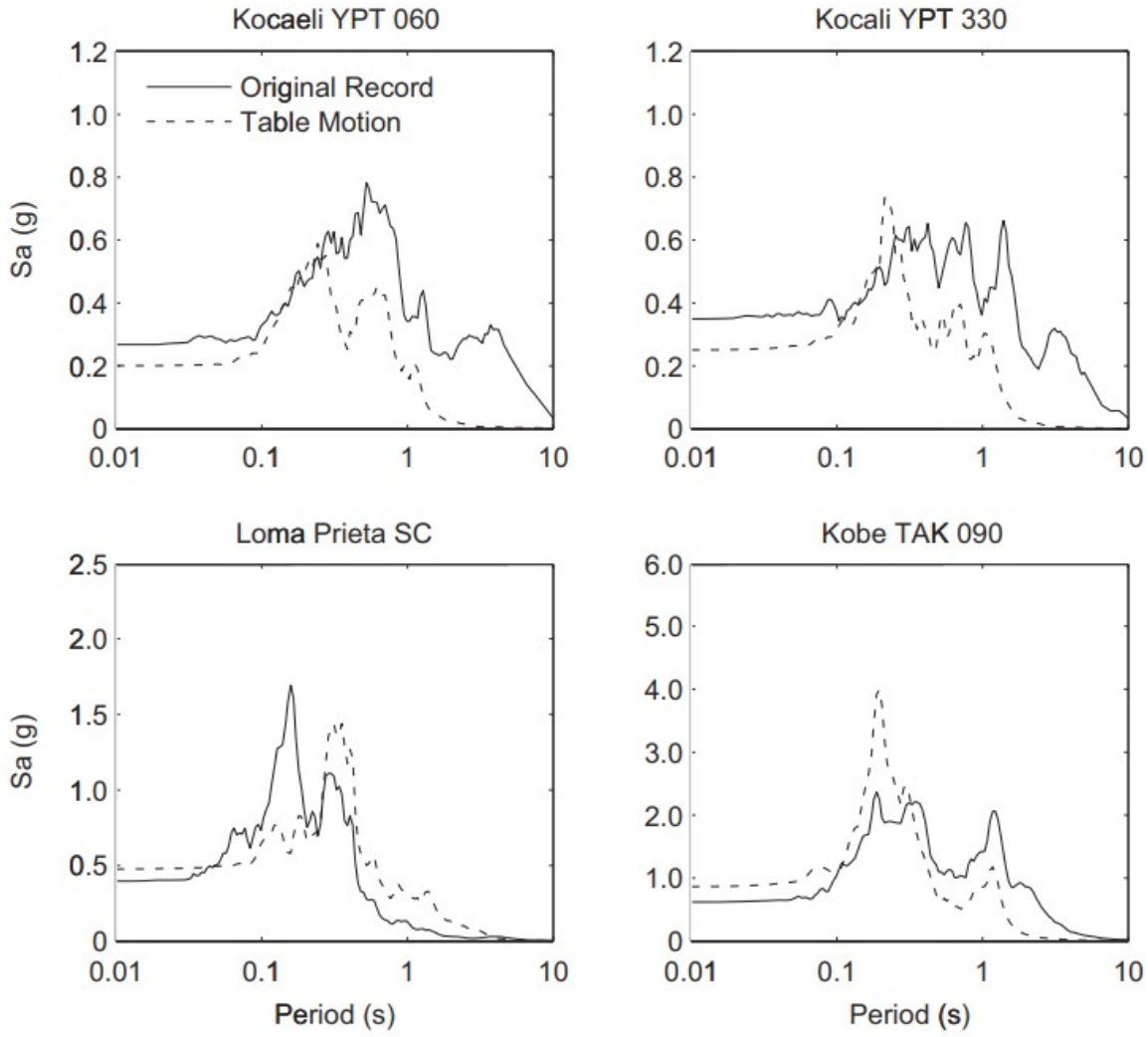

Fig. 3. Recorded and centrifuge-generated ground motions.

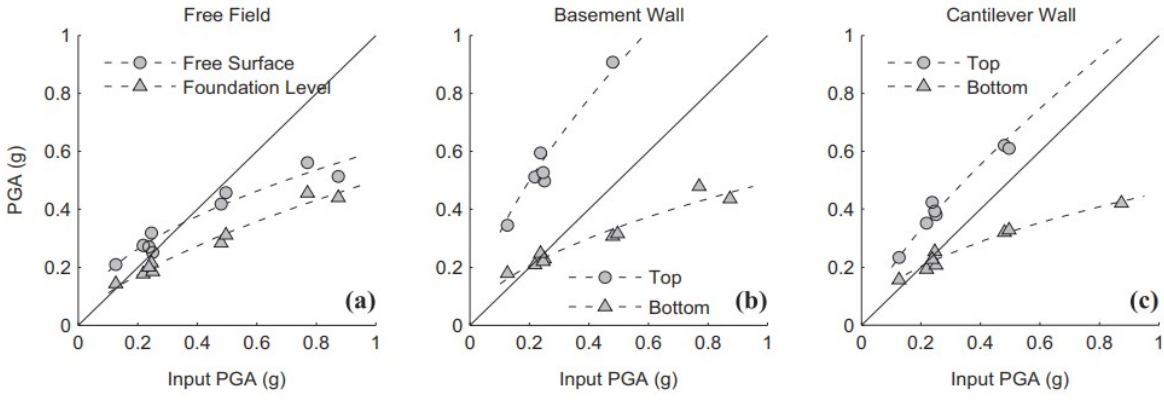

Fig. 4. Ground motion amplification.

4.1. Seismic earth pressures

Fig. 7 shows the history of the pressure sensors readings (raw data in volts) without any baseline correction. Likewise, Fig. 8 shows the distributions of static and maximum dynamic earth pressures for three shaking table motions. Although problems were encountered in adjusting the baseline of pressure sensors, the readings increases approximately linearly with depth and no 'inverted-triangle' distributions are apparent from the data. Thus, the point of application of the total seismic load and dynamic load increments is considered to act at 0.33 H above the base. The magnitude of earth pressures in the cantilever wall was backcalculated from the strain gages located at the base of the wall. In the case of basement walls the magnitude of earth pressures was determined from the load cells and the inertial forces computed from the accelerometers. The immediate consequence of a linearly increasing earth pressure is that the seismic overturning moments are 50% of those predicted by classic methods of analysis [33]. This result is consistent with the experimental response of retaining structures that are founded on soil [20,22].

4.2. Response of the basement wall

The basement compression P_{tot} was computed by adding the loads measured by the six load cells. Using D'Alambert's principle and equilibrium in the horizontal direction, the forces developed at the soil-wall face interfaces are

$$P_{ae}^{south} = P_{tot} - \Delta P_{in}$$
$$P_{ae}^{north} = P_{tot} + \Delta P_{in} \qquad (2)$$

where $\Delta P_{in} = -mH(\ddot{u}_{bottom} + \ddot{u}_{top})/2$ is the inertial load derived from accelerometers located on the basement walls. The static component of the load was removed using a high-pass filter, and then, the dynamic load increments in the south and north walls can be described by

$$\Delta P_{ae}^{south} = \Delta P_{tot} - \Delta P_{in}$$
$$\Delta P_{ae}^{north} = \Delta P_{tot} + \Delta P_{in} \qquad (3)$$

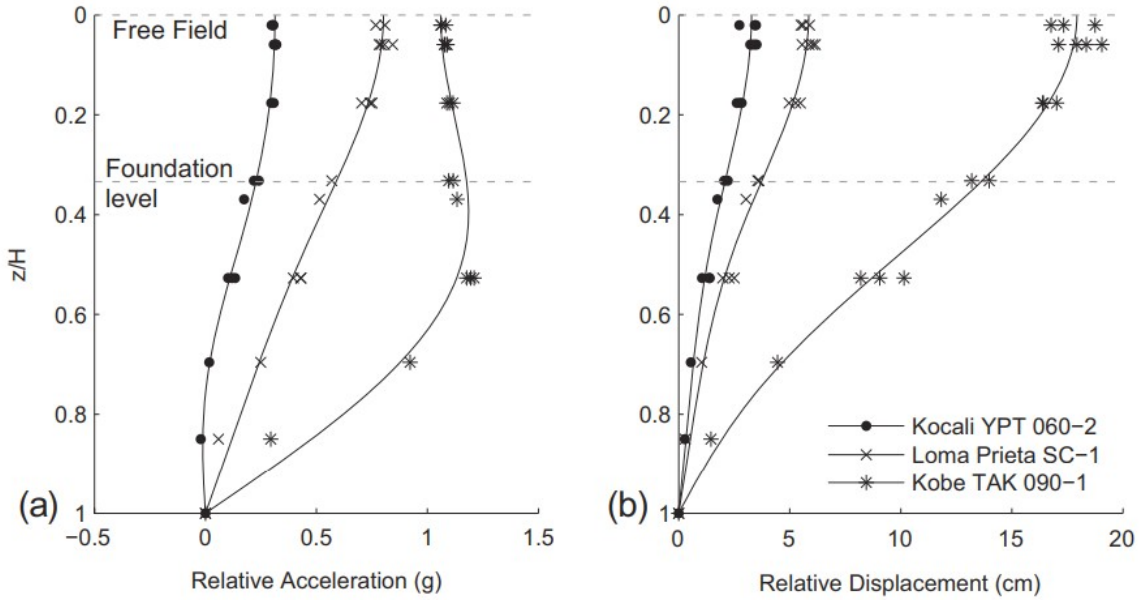

Fig. 5. (a) Maximum acceleration and (b) maximum displacement relative to the model base. Depth z normalized to model depth H = 19.5 m.

This equilibrium analysis shows that the basement compression terms P_{tot} and ΔP_{tot} are the average of the soil-induced loads on the walls and carry no information with regards to the inertial forces. Fig. 9 shows the history of the load increments on the basement in response to the Loma Prieta ground motion. As shown in Fig. 9(a), the inertial loads act in the direction opposite to the acceleration; thus, a positive acceleration increases the dynamic loads on the south wall and reduces the dynamic loads on the north wall and vice versa. Similarly, the compression release in the basement is preceded by positive peaks of inertial loads, which increases the active loads on the north wall. The phase difference between the basement compression and the inertial loads is approximately 0.12 s, which matches the natural period of the retained soil. The dynamic load increments on the south and north walls are shown in Fig. 9(b). As expected, when the load on the south wall is near a local maximum, the load on the north wall is near a local minimum.

A similar behavior was observed for all the ground motions simulated in the centrifuge. Based on a triangular lateral earth pressure distribution, the maximum dynamic load, i.e. $\Delta P_{ae} = \max(|\Delta P_{ae}^{north}|, |\Delta P_{ae}^{south}|)$, was normalized by $0.5\gamma H^2$ and it was found to increases approximately linearly with the free-surface PGA in free field, denoted from here on as PGA_{ff}. Thus, a simple equation is proposed to relate the coefficient of dynamic earth pressure $\Delta K_{ae} = 2\Delta P_{ae}/\gamma H^2$ and the ground acceleration.

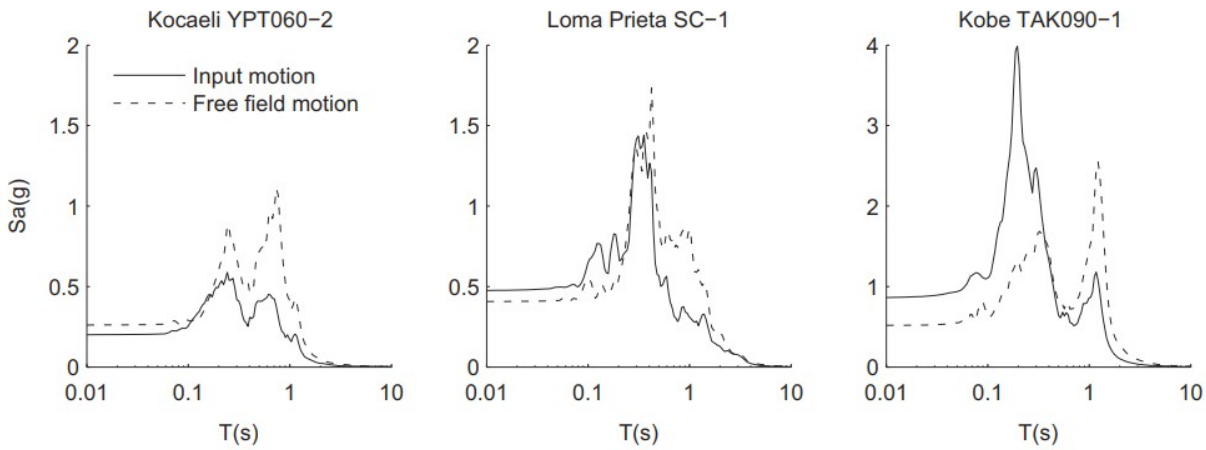

Fig. 6. Acceleration response spectra (ξ=5%) recorded in the soil.

$$\Delta K_{ae}=0.67\left(\frac{PGA_{ff}}{g}-0.10\right)\pm 0.08 \quad (4)$$

In Eq. (4), the term ±0.08 represents the 95% confidence bounds. Note that the equation for the upper-confidence bound can be approximated as $\Delta K_{ae}\approx 0.67 PGA_{ff}/g$, which is equivalent to the Seed and Whitman method [33] with k_h taken as 90% of the design ground acceleration and the resultant applied at 0.33 H.

4.3. Response of cantilever wall

The shear force at the base of the stem on the cantilever wall Q_b was back-calculated using a cubic interpolation of the strain measurements with depth, as described in Eq. (5).

$$Q_b=\frac{3ES}{H}\epsilon(0,t) \quad (5)$$

where ε(0,t) is the bending strain extrapolated at the base of the stem, $S=th^3b/6$ is the wall section modulus, and E is Young's modulus of aluminum. Based on the horizontal equilibrium of the stem and after removing the static components of Q_b, the dynamic load increment on the wall-soil interface is

$$\Delta P_{ae}=\Delta Q_b-\Delta P_{in} \quad (6)$$

where $\Delta P_{in}=-mH(2\ddot{u}_{bottom}+\ddot{u}_{top})/3$ is the wall inertial based on the quadratic distribution of the acceleration. The history of dynamic loads in response to the Loma Prieta motion is presented in Fig. 10, with time shown in prototype scale. A close examination of the load histories, showed that peaks in the inertial load occur in average 0.07 s before peaks in the dynamic load increment ΔP_{ae} because the vertically propagating shear waves

travel faster through the stem than through the retained soil. These observations were common to all the ground motions considered in the experiment.

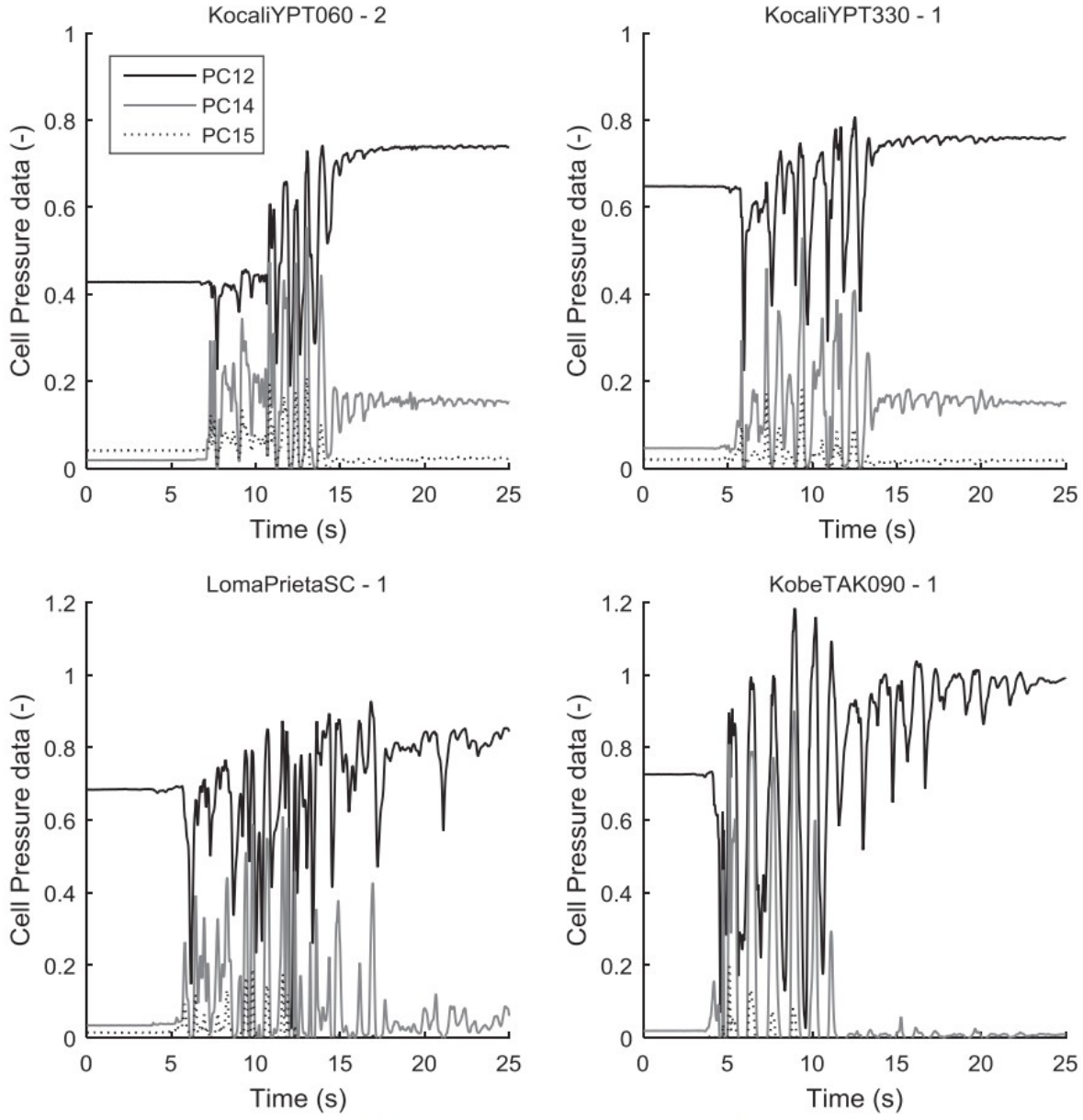

Fig. 7. History of pressure sensors readings (raw data) in the cantilever wall.

The coefficient of dynamic earth pressure $\Delta K_{ae}=2\Delta P_{ae}/\gamma H^2$ was computed for all ground motions and was found to increase monotonically with the surface acceleration at free field. Based on a linear regression of the data, the mean ΔK_{ae} values and their confidence bounds are given in Eq. (7) as a function of PGA_{ff}. Because the cantilever experienced residual rigid-body displacements, the average dynamic earth pressure was 60% smaller than that for the basement walls, which only exhibited transient racking deformations. Although no active wedges were observed in the backfill, the retained soil

followed the cantilever wall and deformed plastically. Also note that the upper-confidence bound to the experimental data approaches the Seed and Whitman [33] solution if 55% of the design acceleration is used.

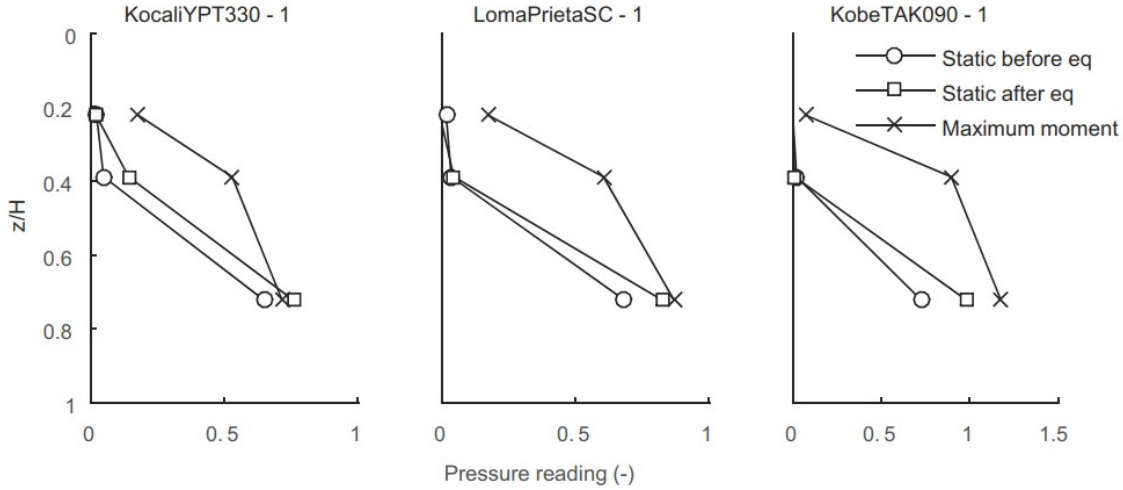

Fig. 8. Earth pressure distributions (raw data) in the cantilever walls recorded before the earthquake, after the earthquake, and at the time of maximum bending moment.

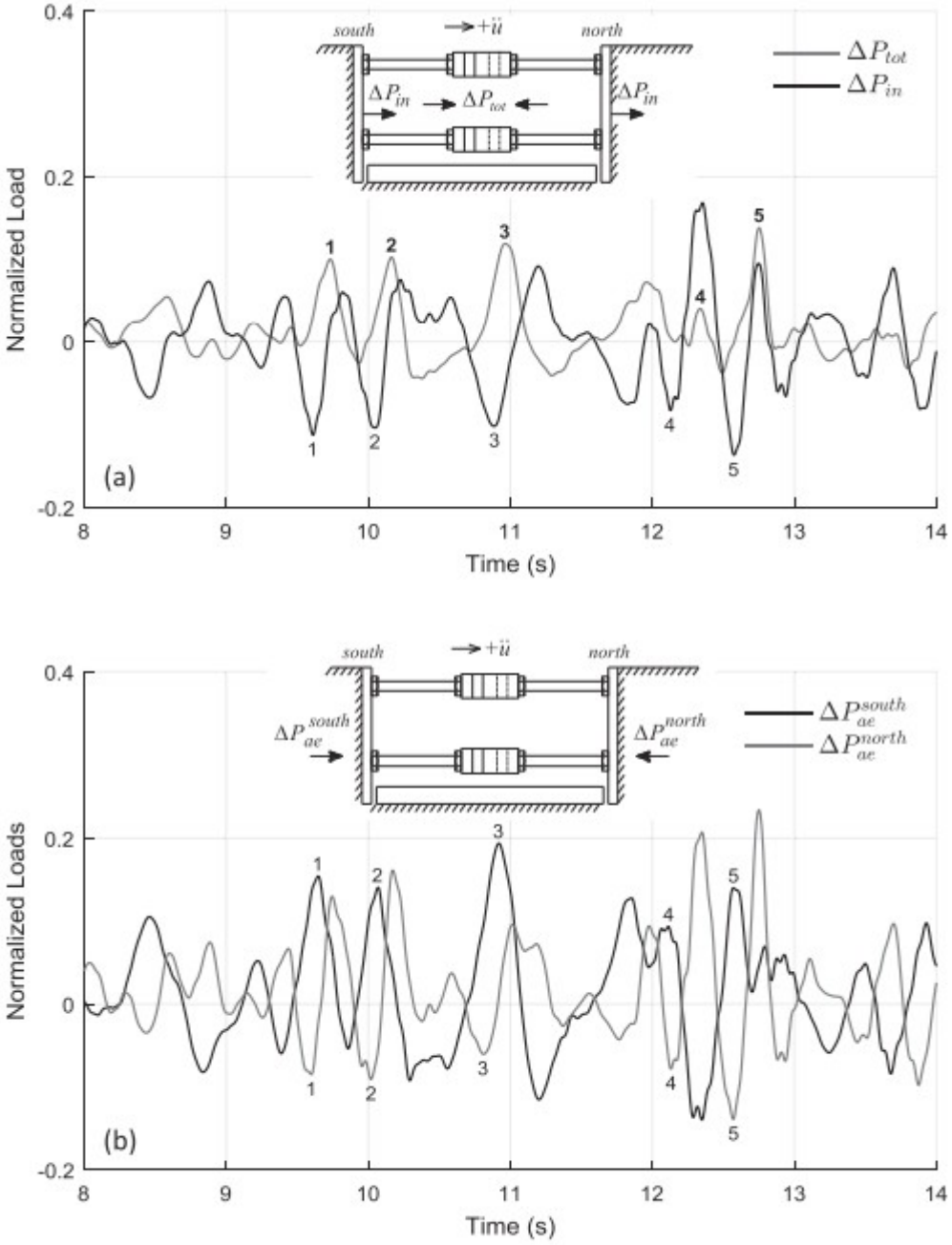

Fig. 9. Dynamic loads on the basement wall during Loma Prieta SC-1 (a) basement compression and inertial loads, and (b) dynamic load increments on the north and south walls. Load values normalized by $1/2\gamma H^2 = 386$ kN/m.

$$\Delta K_{ae} = 0.42\left(PGA_{ff}/g - 0.10\right) \pm 0.05 \qquad (7)$$

From Fig. 10 it was also observed that the peaks of shear force increments ΔQ_b are in average 25% higher than the peaks of dynamic load ΔP_{ae}, thus, for design purposes the maximum bending moment at the base of the stem can

be evaluated simply by increasing in 25% the coefficient of lateral earth pressure from Eq. (7). Overall, these dynamic load increments are significantly smaller than the solutions by Okabe [1] or M-O [2] with a design acceleration of 100% PGA. The apparent conservatism of current design methods have led practicing engineers to use an effective ground acceleration equal to 50% PGA.

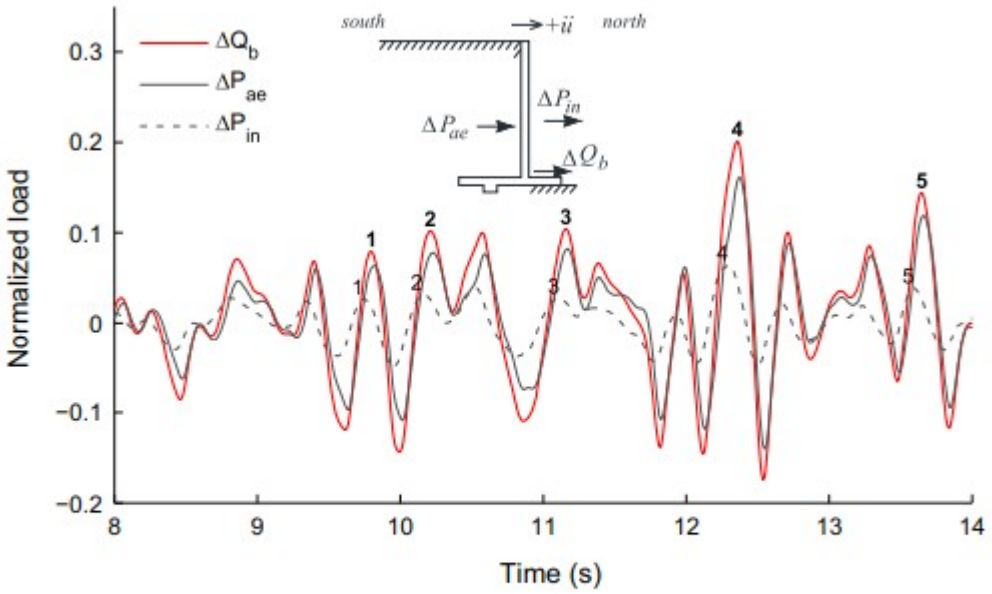

Fig. 10. Shear force at the base of the stem ΔQ_b, soil-induced load ΔP_{ae} and wall inertial load ΔP_{in} during Loma Prieta SC-1. Load values normalized by $1/2\gamma H^2 = 386 kN/m$.

The interpreted coefficients of dynamic load increment are shown in Fig. 11 and compared with traditional methods developed for walls that are founded directly on rock. The current experimental data show that the flexibility of the supporting soil helps reduce the seismic loads developed on the structures. Additionally, these results show that the dynamic loads on the studied basement are not significantly larger than those on the cantilever wall; therefore, in basement walls that may exhibit some degree of racking the use of Wood's [12] solution is considered overly conservative. Instead, the semi-empirical relation by Seed and Whitman [33] with the resultant applied at 0.33 H is a reasonable approach. Another important aspect is the influence of cohesion and soil formation; while these parameters have a marked effect on the initial static earth pressure, experiments conducted with pluviated dry sand with Dr¼75% [20,22] reported similar values of dynamic load increments, in which Eqs. (4) and (7) are still applicable.

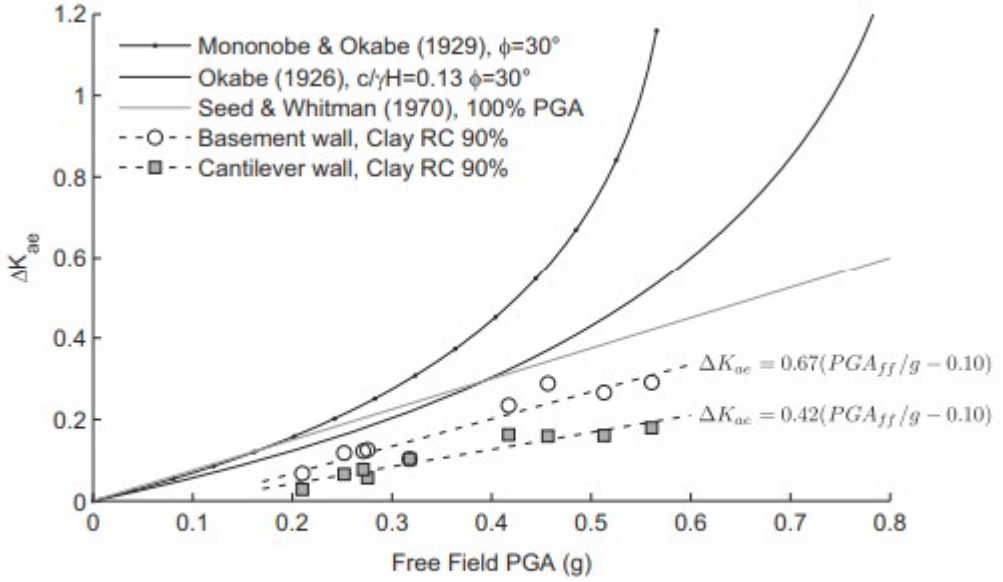

Fig. 11. Coefficient of dynamic earth pressure versus free-field PGA: summary of centrifuge data and limit state solutions.

4.4. Dynamic displacements and deflections

A summary of the rigid-body displacements, basement racking and stem deflections are shown in Fig. 12. The maximum dynamic displacements measured in the free field are also shown for reference. The structure deformations and the shear strain profiles in the soil indicate that the full active conditions were mobilized. No evidence of gapping was observed in the structures except for cantilever wall during Kobe. In both structures, the Kobe ground motions control the response at large accelerations, and thus, the total dynamic displacements increase non-linearly with PGA_{ff}. However, the basement racking and the stem deflection in the cantilever wall increase linearly with PGA_{ff} and account for 30% of the absolute displacement. Residual rigid-body translation in the basement wall was negligible, whereas the cantilever wall exhibited small residual displacements on the order of 3 mm per earthquake (in prototype scale).

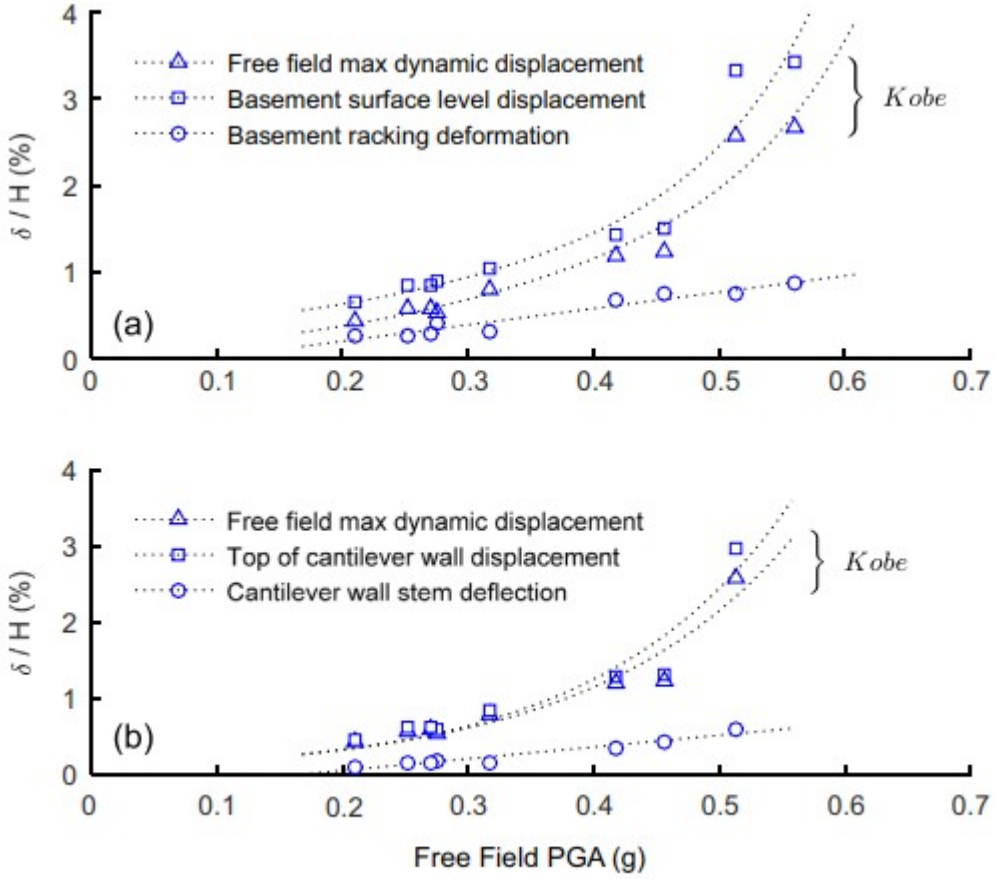

Fig. 12. (a) Dynamic displacements of free-field and basement wall and (b) dynamic displacements of the free-field and cantilever wall.

5. Concluding remarks

The seismic response of a 6-m embedded basement and a 6-m standard cantilever wall with a horizontal cohesive backfill was modeled in a geotechnical centrifuge. The models were built on a 1/36 scale and tested at a centrifuge acceleration of 36*g*. Several instruments were used to measure the seismic interaction between the structures and soil. From the experimental results, the following general conclusions can be drawn:

- The natural soil cohesion and compaction-induced stresses greatly reduce the initial contact stresses between the wall and soil, and in general, there is no amenable way to estimate them accurately. As a result, the total seismic load (static plus dynamic components) is reduced. The dynamic loads, however, are not significantly affected by cohesion or compaction. Similar magnitudes of the dynamic load increments have been observed in recent centrifuge experiments conducted in dry pluviated sand [22].
- Important differences between the measured and expected seismic earth pressures were observed. As stated earlier, the standard design

practice is to assume that the dynamic earth pressures increase towards the surface. This assumption is a direct consequence of the scaling limitations and the experimental setup of typical 1-g shaking tables, where the structures are fixed to a rigid base. However, in the present centrifuge experiments, the basement and cantilever walls were founded on soil rather than a rigid boundary, and the dynamic earth pressures increase approximately linearly with depth.

- The present basement model relied on bracing elements with load cells to capture the average dynamic earth pressure coming from both sides. Although this model was sufficiently rigid against pure horizontal compression, racking deformations were not completely avoided. Thus, strictly speaking, the present results apply to braced excavations or closed culverts that may undergo some degree of racking. The seismic earth pressures on rigid basements with transverse shear walls require further analysis.
- Similar to the basement walls, the seismic load increments measured on the cantilever wall increased linearly with the free-field acceleration and can be approximated as $\Delta K_{ae}=0.42\ (PGA_{ff}/g-0.10)$ and the resultant applied at 0.33 H.

The results presented in this study are applicable to 6 m tall cantilever walls and braced basement walls founded on compacted silty clay, with the ground motion applied perpendicular to the wall. While these results capture the essential features of seismic wall-soil interaction, more experimental data or field data is required to extend the current results to different boundary conditions and wall configurations.

Acknowledgements

Financial support for this study was provided by NSF-NEES under grant CMMI-0936376 and the State of California Department of Transportation under grant No. 65N2170. Additional funding was provided by Facultad de Ingeniería of Universidad del Desarrollo, and the National Research Center for Integrated Natural Disaster Management CONICYT/FONDAP/15110017. Their support is gratefully acknowledged.

References

[1] Okabe S. General theory of earth pressure. J Jpn Soc Civ Eng 1926;12(1):311.

[2] Mononobe N, Matsuo M. On the determination of earth pressures during earthquakes. Proc World Eng Congr 1929;9:179–87.

[3] Prakash S, Saran S. Static and dynamic earth pressures behind retaining walls. In: Proceedings of the Third Symposium on Earthquake Engineering, Vol. 1. Roorkee, India: University of Roorkee; 1966. p. 277–288.

[4] Das BM, Puri VK. Static and dynamic active earth pressure. Geotech Geol Eng 1996;14(4):353–66.

[5] Steedman RS, Zeng X. The influence of phase on the calculation of pseudostatic earth pressure on a retaining wall. Geotechnique 1990;40(1):103–12.

[6] Richards R, Shi X. Seismic Lateral Pressures in Soils with Cohesion. J Geotech Eng 1994;120(7):1230–51 ASCE.

[7] Chen WF, Liu XL. Limit analysis in soil mechanics. Vol. 52. Elsevier; 2012.

[8] Shamsabadi A, Xu SY, Taciroglu E. A generalized log-spiral-Rankine limit equilibrium model for seismic earth pressure analysis. Soil Dyn Earthq Eng 2013;49:197–209.

[9] Brandenberg SJ, Mylonakis G, Stewart JP. Kinematic framework for evaluating seismic earth pressures on retaining walls. J Geotech Geoenviron Eng 2015:04015031.

[10] Matsuo H, O'Hara S. Lateral earth pressure and stability of quay walls during earthquakes. In: Proceedings, Earthquake Engineering, Second World Conference. Tokyo, Japan; 1960. p. 1.

[11] Scott RF. Earthquake-induced pressures on retaining walls. In: Proc. 5th World Conf. on Earthquake Engineering. 1973. p. 1611–1620.

[12] Wood JH. Earthquake induced soil press ures on structures (Ph.D. Thesis).Pasadena, CA: California Institute of Technology; 1973.

[13] Veletsos AS, Younan AH. Dynamic soil pressures on rigid vertical walls. Earthq Eng Struct Dyn 1994;23(3):275–301.

[14] Kloukinas P, Langousis M, Mylonakis G. Simple wave solution for seismic earth pressures on nonyielding walls. J Geotech Geoenviron Eng 2012;138(12):1514– 9.

[15] Clough GW, Duncan JM. Finite element analyses of retaining wall behavior. J Soil Mech Found Div 1971;97(12):1657–73.

[16] Seed RB, Duncan JM. FE analyses: compaction-induced stresses and deformations. J Geotech Eng 1986;112(1):23–43.

[17] Nadim F, Whitman R. A numerical model for evaluation of seismic behavior of gravity retaining walls. R82-33. Massachusetts Institute of Technology, Report 1982, 232p (480 S43 no.2 1982), 1982.

[18] Green RA, Olgun CG, Cameron WI. Response and modeling of cantilever retaining walls subjected to seismic motions. Comput-Aided Civ Infrastruct Eng 2008;23(4):309–22.

[19] Gazetas G, Psarropoulos PN, Anastasopoulos I, Gerolymos N. Seismic behaviour of flexible retaining systems subjected to short-duration moderately strong excitation. Soil Dyn Earthq Eng 2004;24(7):537–50.

[20] Al Atik L, Sitar N. Seismic earth pressures on cantilever retaining structures. J Geotech Geoenviron Eng 2010;136(10):1324–33.

[21] Sitar N, Mikola RG, Candia G. Seismically induced lateral earth pressures on retaining structures and basement walls. In: Proceedings of Geotechnical Engineering State of the Art and Practice, GeoCongress. 2012. p. 335–358.

[22] Mikola RG, Sitar N. Seismic earth pressures on retaining structures in cohesionless soils. UCB/GT-2013-01, University of California, Berkeley, Geotechnical Engineering. 2013. ⟨nisee.berkeley.edu/documents/elib/www/documents/ GEOTECH/UCB-GT-2013-01.pdf⟩.

[23] Candia Agusti G, Sitar N. Seismic earth pressures on retaining structures with cohesive backfills. UCB/GT-2013-02, University of California, Berkeley, Geotechnical Engineering. 2013. ⟨nisee.Berkeley.edu/documents/elib/WWW/docu ments/GEOTECH/UCB-GT-2013-02.PDF⟩.

[24] Clough GW, Fragaszy RF. A study of earth loadings on floodway retaining structures in the 1971 San Fernando Valley earthquake. In: Proceedings of the Sixth World Conference on Earthquake Engineering, Vol. 3. 1977.

[25] Verdugo R, Sitar N, Frost JD, Bray JD, Candia G, Eldridge T, Urzua A. Seismic performance of earth structures during the February 2010 Maule, Chile, earthquake: dams, levees, tailings dams, and retaining walls. Earthq Spectra 2012;28(S1):S75–96.

[26] Rollings K, Ledezma C, Moltalva G. Geotechnical aspects of April 1st 2014, M8.2 Iquique Earthquake. Geotechnical Extreme Event Reconnaissance Association (GEER). 2014. ⟨http://www.geerassociation.org/⟩.

[27] Candia G, Sanhueza C, Sitar N. Evaluación del empuje sísmico en muros de contención en base a un perfil de aceleraciones de campo libre.Santiago, Chile: VIII Congreso Chileno DE Ingeniería Geotécnica; 2014. p. 2014.

[28] Jacobson PN. Translational behavior of gravity retaining walls during earthquakes. Res Rep 1980:80–9 (University of Canterbury, New Zealand).

[29] Matsuo H. Experimental study on the distribution of earth pressures acting on a vertical wall during earthquakes. J Jpn Soc Civ Eng 1941;27(2).

[30] Matsuo H, O'Hara S. Dynamic pore water pressure acting on quay walls during earthquakes. In Proceedings of the Third World Conference on Earthquake Engineering, Vol. 1. 1965. p. 130–140.

[31] Sherif MA, Fang YS. Dynamic earth pressures on walls rotating about the top. Soils Found 1984;24(4):109–17.

[32] Sherif MA, Ishibashi I, Lee CD. Earth pressure against stiff retaining walls. J Geotech Eng, 108. ASCE; 1982. p. 679–95.

[33] Seed HB, Whitman RV. Design of earth retaining structures for dynamic loads. ASCE Specialty Conference, Lateral Stresses in the Ground and Design

of Earth Retaining Structures. Ithaca, New York: Cornell Univ.; 1970. p. 103–147.

[34] Kutter BL. Recent advances in centrifuge modeling of seismic shaking. In: Third International Conference on Recent Advances in Geotechnical Earthquake Engineering and Soil Dynamics (1981: April 2-7; St. Louis, Missouri). Missouri S&T (formerly the University of Missouri–Rolla), 1995.

[35] Ortiz LA, Scott RF, Lee J. Dynamic centrifuge testing of a cantilever retaining wall. Earthq Eng Struct Dyn 1983;11:251–68.

[36] Bolton MD, Steedman RS. Centrifugal testing of micro-concrete retaining walls subject to base shaking. In: Proceedings of Conference on Soil dynamics and Earthquake Engineering, Southampton, Vol. 1. Balkema; 1982. p. 311–329.

[37] Bolton MD, Steedman RS. The behavior of fixed cantilever walls subject to lateral shaking. In: Proceedings of Symposium on the Application of Centrifuge Modeling to Geotechnical Design. Balkema: University of Manchester; 1984. p. 302–314.

[38] Dewoolkar MM, Ko HY, Pak RY. Seismic behavior of cantilever retaining walls with liquefiable backfills. J Geotech Geoenviron Eng 2001;127(5):424–35.

[39] Nakamura S. Reexamination of Mononobe-Okabe theory of gravity retaining walls using centrifuge model tests. Soils Found 2006;46(2):135–46.

[40] Anderson DG, Martin GR, Lam I, Wang JN. Seismic analysis and design of retaining walls, slopes and embankments, and buried structures. NCHRP Rep 2008:611.

[41] Shukla SK, Gupta SK, Sivakugan N. Active earth pressure on retaining wall for c-ϕ soil backfill under seismic loading condition. J. Geotech. Geoenviron. Eng. 2009.

[42] Darandeli M. Development of a new family of normalized moduli reduction and material damping curves (Ph.D. Thesis) (Doctoral dissertation).Austin: University of Texas at Austin; 2001.

[43] Sun JI, Golesorkhi R, Seed HB. Dynamic moduli and damping ratios for cohesive soils. Earthquake Engineering Research Center, University of California; 1988.

[44] Seed RB, Chang SW, Dickenson SE, Bray JD. Site-dependent seismic response including recent strong motion data. In: Proc., Special Session on Earthquake Geotechnical Engineering, XIV Int. Conf. on Soil Mech. and Found. Eng. Hamburg: AA Balkema Publ; 1997. p. 125–134.

[45] Gazetas G. Vibrational characteristics of soil deposits with variable wave velocity. Int J Numer Anal Methods Geomech 1982;6(1):1–20.